Science Advances
AAAS

Supplementary Materials for

The Integrator complex regulates microRNA abundance through RISC loading

Nina Kirstein *et al.*

Corresponding author: Ramin Shiekhattar, rshiekhattar@med.miami.edu

Sci. Adv. **9**, eadf0597 (2023)
DOI: 10.1126/sciadv.adf0597

The PDF file includes:

Other Supplementary Material for this manuscript includes the following:

Fig. S1.

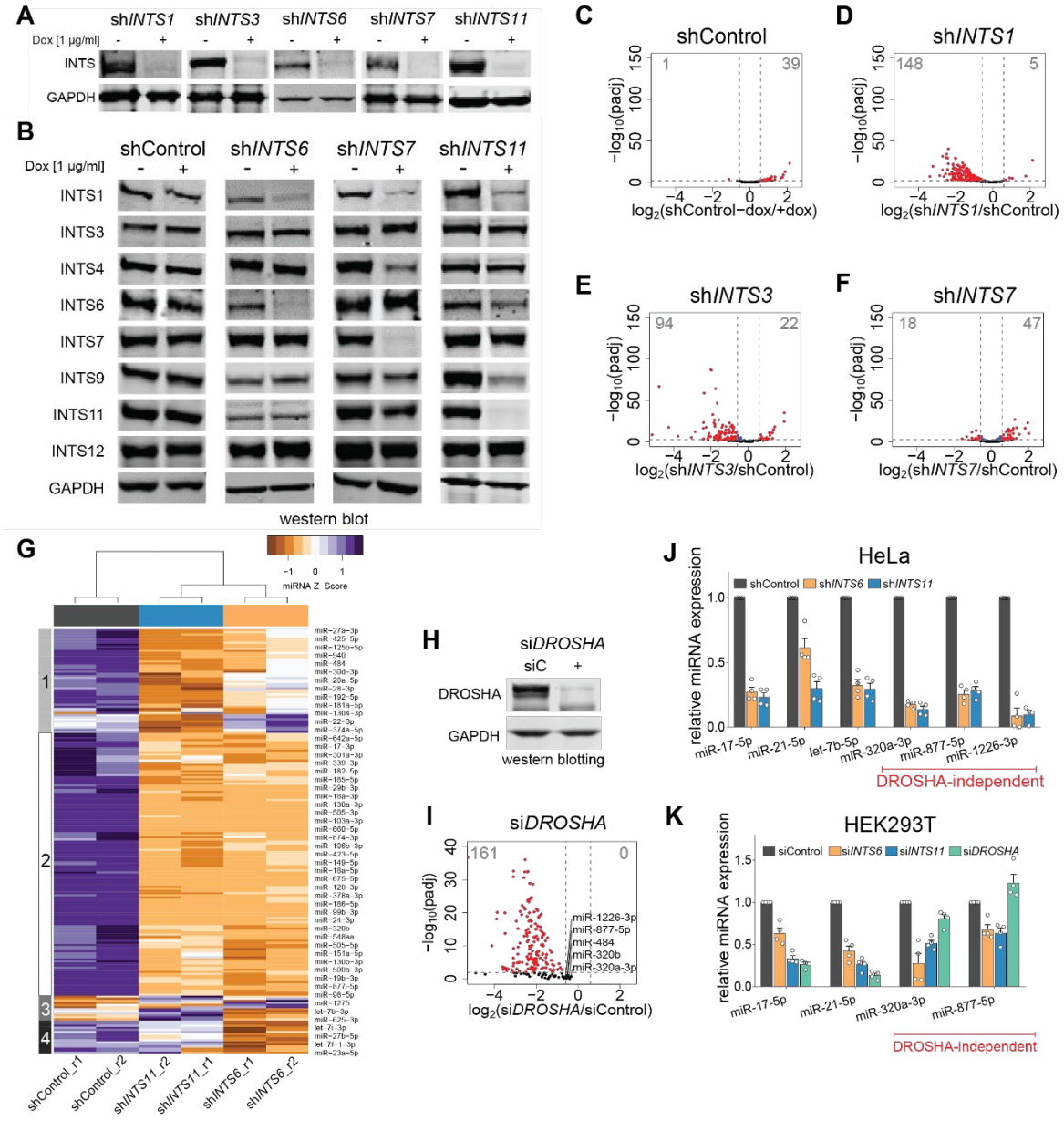

Fig. S1. DROSHA-independent miRNAs are down-regulated after INTS knock-down. (**A**) Immunoblot detection of successful knock-down of INTS1, INTS3, INTS6, INTS7, and INTS11 before and after shRNA induction with Doxycyclin (Dox) at 1 µg/ml. GAPDH was used as loading control. (**B**) Immunoblot of shControl before and after induction using the same INTS antibodies. (**C-F**) Volcano plot comparing statistical significance and miRNA $\log_2$ fold change between

control and knock-down cells. Padj refers to adjusted *P*-value as calculated by DESeq2. Significantly regulated miRNAs are depicted in red. **c**, Uninduced shControl compared to induced shControl. (**D**) Sh*INTS1* compared to induced shControl. (**E**) Sh*INTS3*. (**F**) Sh*INTS7*. (**G**) Heat map of normalized miRNA expression from shControl, sh*INTS6*, and sh*INTS11* (Z-score of normalized read counts per row). Column and row orders were determined by unsupervised hierarchical clustering. (**H**) Immunoblot detection of DROSHA after siRNA knock-down in HeLa. (**I**) Volcano plot comparing statistical significance and miRNA $\log_2$ fold change between siControl and si*DROSHA* knock-down HeLa cells. Significantly regulated miRNAs are depicted in red. DROSHA-independent miRNAs are indicated. (**J, K**) Relative miRNA expression levels in (**J**) HeLa shControl, sh*INTS6*, and sh*INTS11* cells, or (**K**) HEK293T cells transfected with siControl, si*INTS6*, si*INTS11*, or si*DROSHA*. MiRNAs were detected by specific TaqMan probes for the indicated miRNAs and relative miRNA levels were calculated against RNU43 expression and shControl/siControl using ΔΔct method. Mean + SEM, $n = 4$. DROSHA-independent miRNA examples are indicated in red.

Fig. S2.

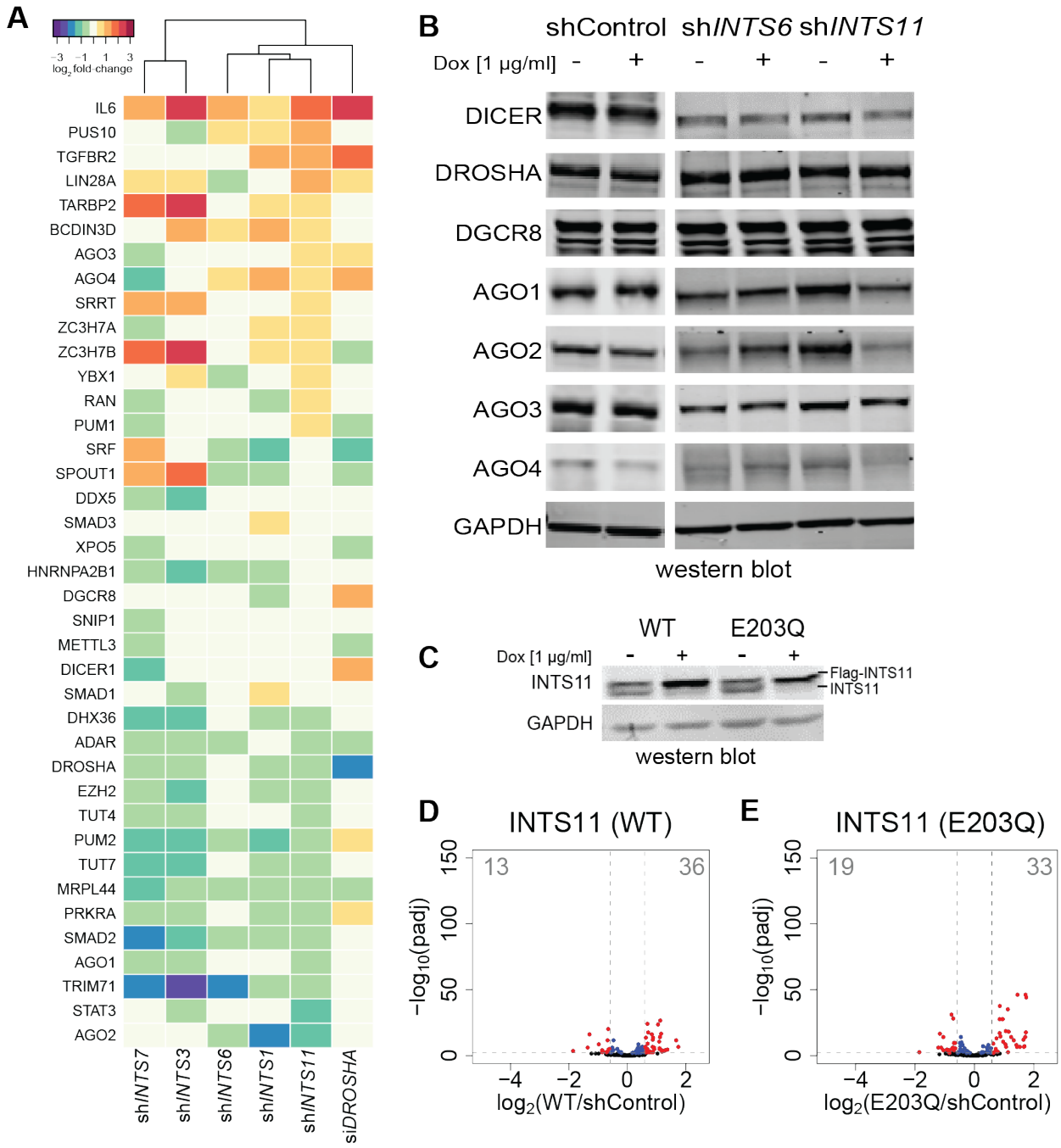

Fig. S2. MiRNA loss does not depend on Integrator's endonucleolytic cleavage activity. (**A**) Heat map of $\log_2$ fold changes in transcription levels of miRNA machinery-related genes after knock-down with the indicated sh/siRNAs calculated against sh/siControl. Gene names related to miRNA machinery were extracted from miRNA-containing Gene Ontology terms. Row order

based on expression changes in sh*INTS11* cells, column order was determined by complete linkage hierarchical clustering. (**B**) Immunoblot detection of the expression of miRNA biogenesis machinery and Argonaute proteins in shControl, sh*INTS6*, and sh*INTS11* cells before and after induction. GAPDH was used as loading control. (**C**) INTS11 Immunoblot of sh*INTS11* cells stably expressing wild type INTS11(WT) or catalytic mutant E203Q with and without shRNA induction. GAPDH was used as loading control. (**D, E**) Volcano plot comparing statistical significance and miRNA $\log_2$ fold change detected by smRNA-seq between shControl and (**D**) WT INTS11, or (**E**) E203Q INTS11 cells in sh*INTS11* knock-down background. Padj refers to adjusted *P*-value as calculated by DESeq2. Significantly regulated miRNAs are depicted in red.

Fig. S3.

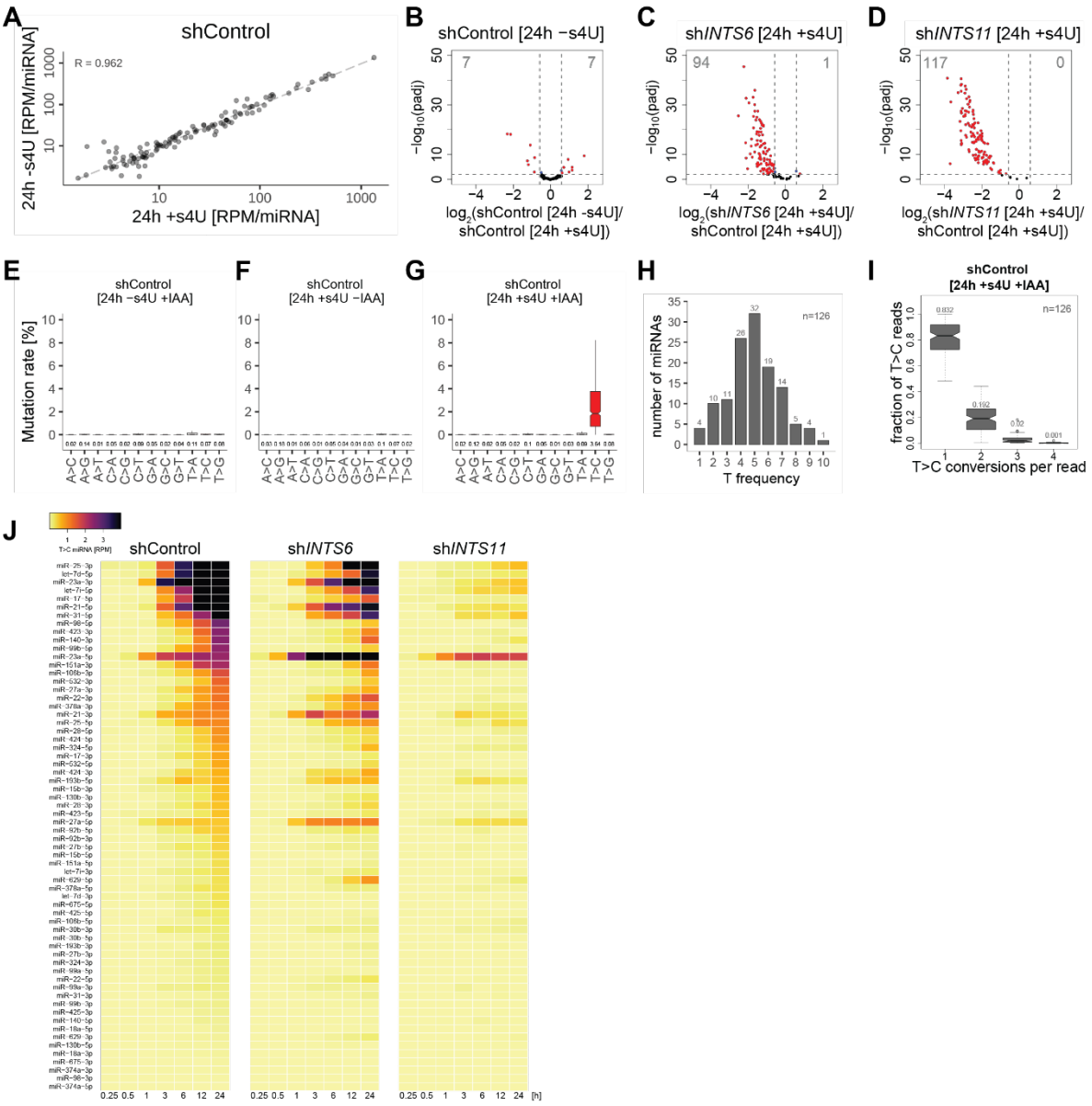

Fig. S3. S4U labeling does not affect miRNA abundance. (**A**) Scatter plot of steady state miRNA abundance [RPM] of 126 miRNAs in shControl samples with and without s4U treatment. Spearman correlation coefficient R is indicated. (**B-D**) Volcano plot comparing statistical significance and miRNA $\log_2$ fold change between shControl cells [24h +s4U] and (**B**) ShControl cells control [24h -s4U]. (**C**) Sh*INTS6* cells [24h +s4U]. (**D**) Sh*INTS11* [24h +s4U]. Padj refers to adjusted *P*-value as calculated by DESeq2. Significantly regulated miRNAs are depicted in red,

their numbers indicated on top. (**E-G**) Conversion rates for every possible nucleotide conversion were detected for the miRNAs (positions 1-18 after background normalization) in shControl after 3d of Doxycycline treatment. (**E**) Without s4U but with iodoacetamide (IAA) [24h –s4U +IAA]. (**F**) [24h +s4U –IAA]. (**G**) [24h +s4U +IAA]. Outliers were removed from representation; mean conversion rates are indicated below. (**H**) Histogram representation of "T" frequency per miRNA in positions 1-18. $n = 126$. (**I**) Boxplot of the frequency of T>C conversion per read and per miRNA ($n = 126$) in shControl cells after 24h s4U labeling and IAA treatment. The median fraction is indicated on top. (**J**) Heatmap representation of the T>C miRNA expression [RPM] of 64 miRNAs (corresponding to 32 guide and passenger miRNA duplexes) during the time course of shControl (left panel), sh*INTS6* (middle panel), and sh*INTS11* (right panel).

Fig. S4.

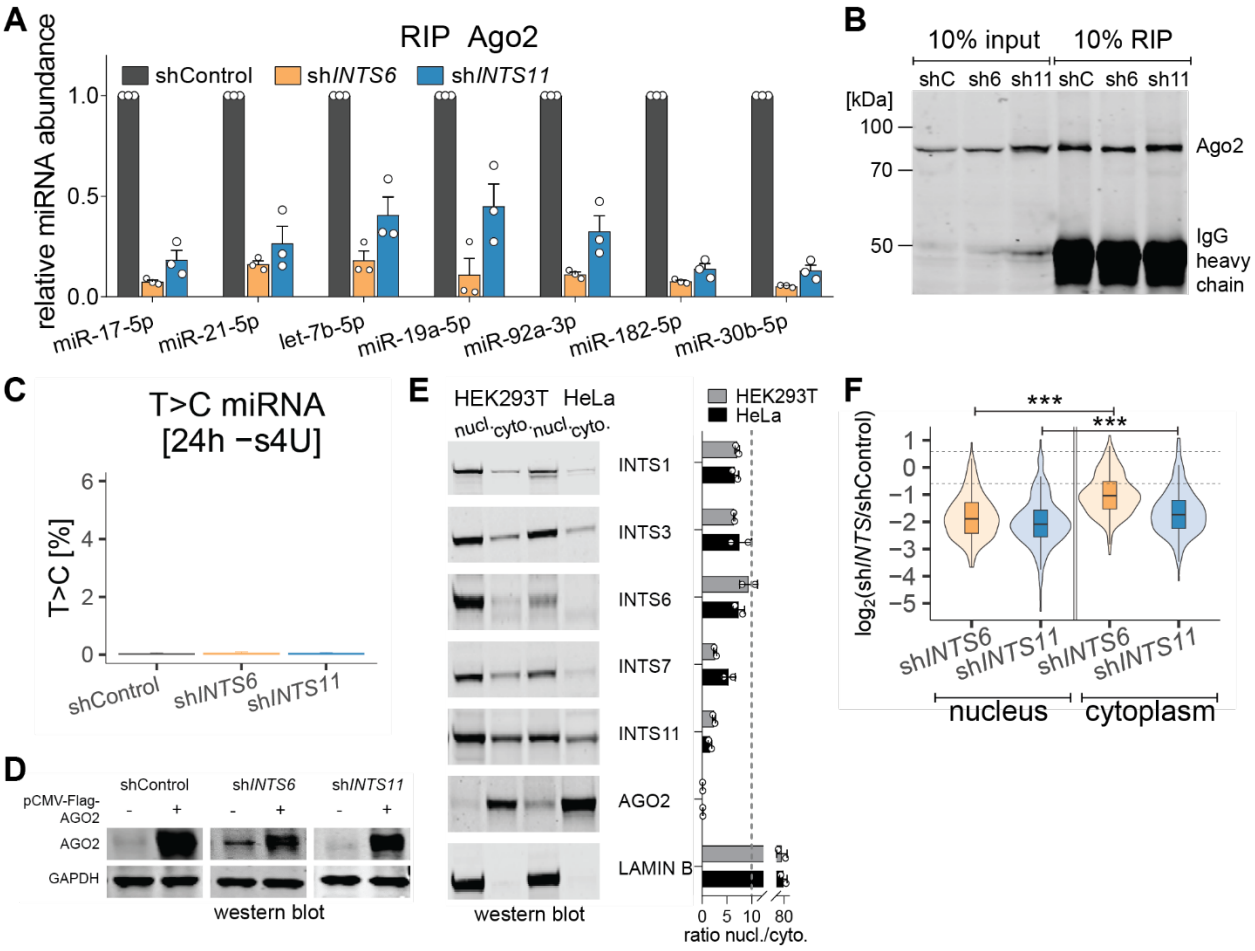

Fig. S4. MiRNA loss is independent of subcellular localization. (**A**) AGO2 RIP from shControl, sh*INTS6*, and sh*INTS11* cells followed by Taqman-qPCR. MiRNA levels were normalized to shControl and ath-miR-159a spike-in. Mean ± SEM, $n = 3$. (**B**) Immunoblot detecting AGO2 after example AGO2 RIP from induced shControl (shC), sh*INTS6* (sh6), and sh*INTS11* (sh11) cells. (**C**) Percentage of T>C labeled miRNAs after AGO2 RIP from induced cells without s4U treatment. Mean ± SEM. (**D**) Immunoblot detection of AGO2 in induced shControl, sh*INTS6*, and sh*INTS11* cells, before and after transfection of pCMV-Flag-AGO2 plasmid. GAPDH servers as loading control. (**E**) Left panel: Immunoblot detecting INTS as indicated from nuclear and cytoplasmic extracts from HEK293T and HeLa cells. LAMIN B serves as nuclear control. Right panel: Signal

quantification and ratio of nuclear signal/ cytoplasmic signal of two independent experiments. (**F**) Box- and violin plot depicting the $\log_2$ fold change of miRNA abundance per subcellular compartment obtained by smRNA-seq in the indicated knock-down cells, calculated against miRNA levels in induced shControl cells. 205 expressed miRNAs quantified by mirdeep2 were taken into account. Statistics were performed using one-way ANOVA followed by Tukey's post-hoc test. ***$P < 0.001$.

Fig. S5.

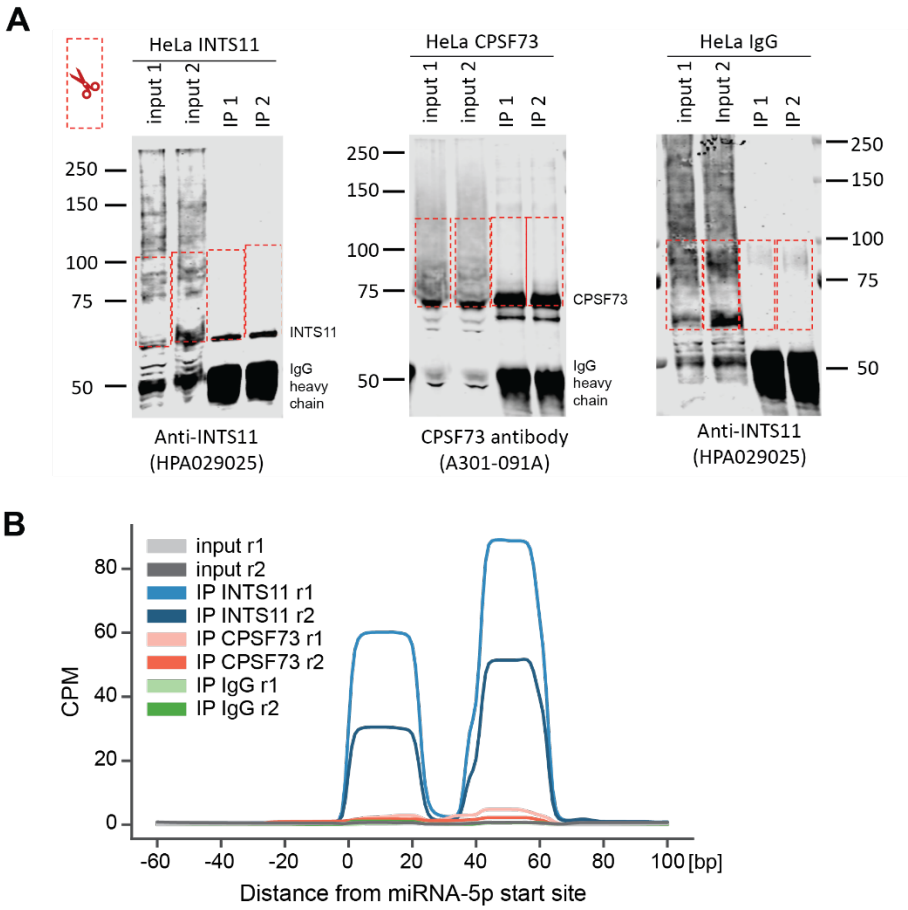

Fig. S5. ECLIP controls and replicate depiction. (**A**) Control IP-western blot for comparing pull down efficiencies of INTS11 and CSPF73 antibodies, including 10% of the input samples. The areas with the relevant protein sizes are indicated by dashed red boxes. (**B**) Global average of INTS11, CPSF73, and IgG eCLIP replicates around 112 5p-miRNAs aligned at their start site.

Fig. S6.

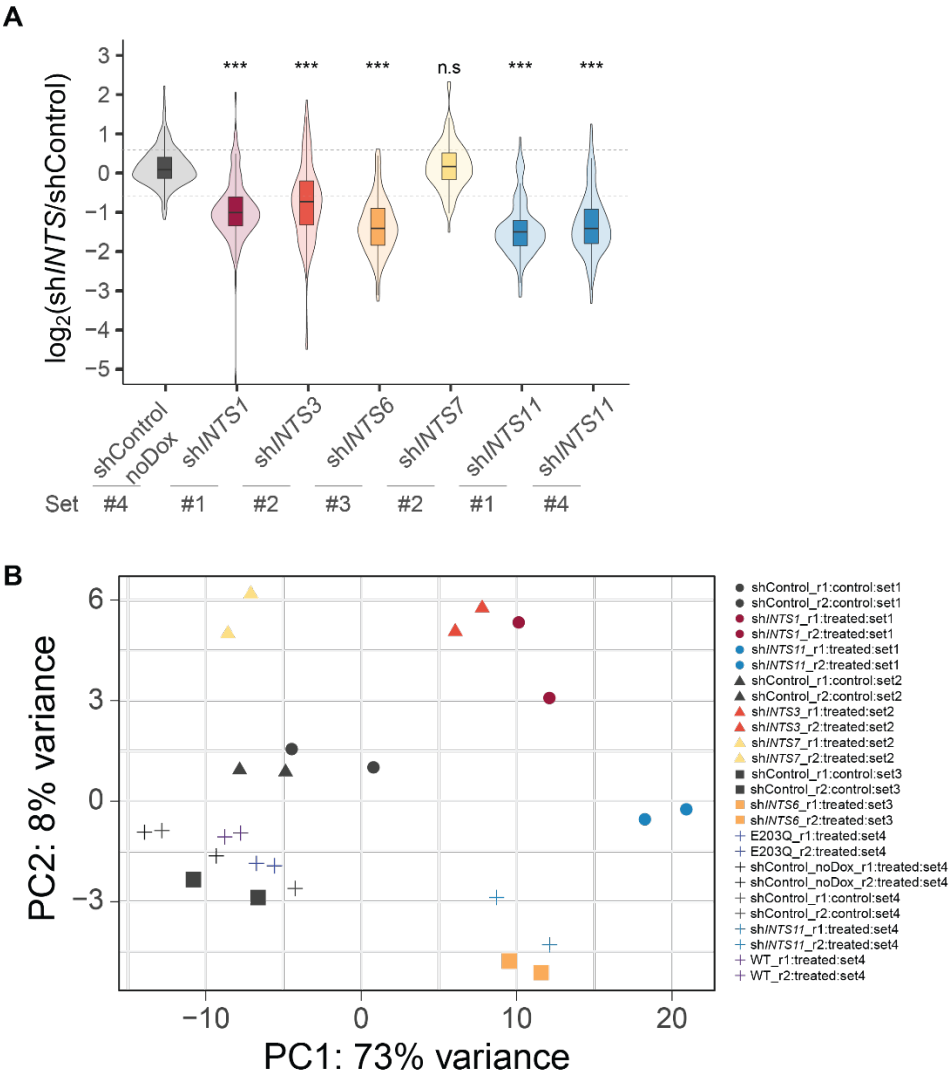

Fig. S6. Validation of individual data sets. (**A**) Box- and violin plot of DESeq2 miRNA (*n* = 205) differential expression based on original data files. Sample replicates of each sequencing set were modeled against their respective control. Sequencing sets are indicated as displayed in Table 1. (**B**) Principal component analysis (PCA) of all samples and sequencing sets based on 205 miRNAs. Color code according samples, symbols refer to sequencing sets.

Table S1.

Detailed list of 205 analyzed miRNAs including RPM, differential expression and eCLIP/RIP coverage. Sheet '205_miRNA_RPM_allSamples' lists RPM results for each merged replicate as calculated by DESeq2. Sheet '205_miRNAs_log2FC_HeLa_allSamples' lists log_2 fold change of each miRNA expression compared to shControl (as depicted in volcano plots). Sheet '205_miRNA_eclip_rip_rpm' depicts RPM-normalized values for each miRNA detected from merged INTS11 eCLIP or AGO2 RIP experiments. MiRNAs that were not captured are indicated as NA.